Generalized density-of-states and anharmonicity of the low-energy phonon bands from coherent inelastic neutron scattering response in the pyrochlore osmates AOs_2O_6 (A=K, Rb, Cs)

Hannu Mutka,* Michael Marek Koza, and Mark Robert Johnson
Institut Laue Langevin, 6 Rue Jules Horowitz, B.P. 156, 38042 Grenoble Cedex 9, France

Zenji Hiroi, Jun-Ichi Yamaura, and Yohei Nagao
Institute for Solid State Physics, University of Tokyo, Kashiwanoha, Kashiwa, Chiba 277-8581, Japan
(Received 22 July 2008; published 30 September 2008)

Inelastic neutron scattering on powder samples has been employed to investigate the lattice dynamics of alkali-metal osmates. We have obtained the neutron weighted generalized phonon density-of-states from momentum-transfer averaged coherent inelastic response. We have paid special attention to the low-energy modes that have been assigned to the Einstein term of the lattice specific heat and from which a "rattling" behavior of the alkali atoms has been inferred. In all of the three compounds our results reveal a split band with two prominent peaks in the low-energy range associated with the vibrational modes of A atoms. The temperature dependence of these bands has been followed in the range from 1.5 K$<T<$300 K. The strongest temperature effect is visible in the case of KOs_2O_6, the split band peaking at $\hbar\omega \approx 5.5$ meV, and 6.8 meV at $T=300$ K softens on cooling resulting in a main band at about $\hbar\omega \approx 3.4$ meV at $T \lesssim 50$ K, while a smaller softening of $\Delta(\hbar\omega)<1$ meV is seen in the other two compounds. In agreement with earlier work the temperature dependent modifications of the phonon spectrum can be attributed to the weak potential felt by the A atom in the oversized cage where it is located. At low T the characteristic energies for each of the compounds are well correlated with the specific-heat observations published earlier. The powder averaged phonon response shows Q dependence indicating coherent coupling of the alkali atom vibrations with the rest of the lattice.

DOI: 10.1103/PhysRevB.78.104307 PACS number(s): 63.20.Ry, 61.05.cf

I. INTRODUCTION

Lattice dynamics of encaged atoms represents a general challenge associated with the "rattling mode" scenario[1] that is often called for in the framework of materials for thermoelectric application such as skutterudites[2,3] and clathrates.[4] A common approach to characterize the lattice dynamics quantitatively has been the analysis of heat capacity alone. However, the exact nature of the "rattling modes" as well as the mechanisms by which they influence the physical properties are somewhat elusive questions that merit detailed investigations on a wide variety of systems. For example recent work on the $(La,Ce)Fe_4Sb_{12}$ skutterudites concluded that quasiharmonic lattice dynamics prevails in these systems.[5,6]

In this context we can note the ongoing research for the understanding the particular properties of the β-pyrochlore alkali-metal osmates. This was triggered by the observations of superconducting properties of these compounds.[7–10] A particular issue of interest is the correlation of the low-energy phonon modes, as detected by specific-heat measurements, with the superconducting critical temperatures. The recent efforts have focused on the KOs_2O_6 compound that has the highest superconducting $T_c=9.6$ K while it displays the lowest characteristic energy of the Einstein mode ($\Theta_E \approx 20 \ldots 40$ K, dependent on the number of Einstein modes used) as deduced from the analysis of the specific heat.[10,11] In the Rb and Cs counterparts ($T_c=6.3$ and 3.3 K, respectively) the existence of Einstein modes at somewhat higher energies ($\Theta_E=60$ and 70 K, respectively) has also been concluded from specific-heat data.[10]

Computational theory work[12,13] has pointed out that the position of the alkali atoms in the oversize cage can lead to large amplitude, even anharmonic, vibrations essentially along the $\langle 111 \rangle$ lattice directions toward neighboring alkali atoms positioned on a diamond sublattice. This tendency is highlighted in the case of potassium atoms in KOs_2O_6. Several reports using a variety of methods have evoked this circumstance as a potentially important factor in the superconducting properties of KOs_2O_6.[14,15] An additional low-T phase transition is seen in single-crystal samples[16] and it has been conjectured that this specific-heat feature could be associated with ordering of the K-atom displacements off the center of the cage.[13] A recent powder-diffraction study proposed experimental evidence for randomly off-centered positions for the K atoms.[17] Anharmonicity of the low-energy phonons as a signature of "rattling" was concluded from T dependence of NMR relaxation[18] which was examined further in a theoretical approach.[19]

To investigate the hypotheses that have emerged in the studies cited above direct evidence of the lattice dynamics and temperature dependence of phonon modes of the AOs_2O_6 compounds is necessary. The first inelastic neutron scattering studies at $T=300$ K found a low-energy response in good agreement with the Einstein mode frequencies of the Rb and Cs compounds, but in the case of KOs_2O_6 the observed mode energy was considerably higher than expected from the low-temperature specific-heat analysis.[20] Similarly the low-energy Raman-active mode associated with the K atom was found at an energy much higher than expected, even at the low-T range.[21] These observations brought up the main motivation for the work reported here. First to gain further experimental information on the issues related to the vibrational dynamics of the osmates, especially in terms of

temperature dependence and second, to examine the aspects relevant to the general problem concerning the "rattling" mode scenario.

Inelastic neutron scattering is certainly the most comprehensive probe for the experimental study of lattice dynamics. With single-crystal samples the phonon dispersions $\hbar\omega(\mathbf{q})$ are conveniently defined in selected regions of interest of the reciprocal space and a full analysis of the intensities can be used for the determination of the eigenmodes. When large enough single crystals are not promptly available polycrystalline powders can be used and with appropriate instruments and state of the art data analysis, the information from such powder averaged observation can be used to understand not only the characteristic energies (density-of-states) but also some wave-vector dependencies that characterize the correlations between the movements of individual atoms, giving the possibility to examine the localized, individual nature of the mode as opposed to more collective behavior coupled with the rest of the lattice.[5] Also the temperature dependence of the dynamic response can be examined over a wide range to detect variations due to lattice instabilities and anharmonicity for example. We have chosen to examine the AOs_2O_6 compounds with this approach, and we report here the first experimental conclusions. These results on the lattice dynamics of β pyrochlores reveal interesting trends that can be directly compared to the existing specific-heat data. The observed details of the temperature dependence and of the characteristic energy features go far beyond the present knowledge based on the analysis of thermodynamic data as well as that acquired in the earlier neutron and Raman spectroscopy results reported recently.[20,21]

In the following, after explanation of the experimental details we shall give an account on the analysis of our coherent inelastic neutron scattering data obtained on the polycrystalline powder samples. We extract the neutron weighted generalized density-of-states within the incoherent approach and examine the temperature dependence of the low-energy phonon bands in the range $1.5\ \mathrm{K} < T < 300\ \mathrm{K}$. We shall also take a look at the Q-dependent response that characterizes the collective vibrations in a powder sample. These experimental results are then discussed in relation with the earlier thermodynamic and spectroscopic observations.

II. EXPERIMENTS AND DATA ANALYSIS

A. Samples and spectrometers

The polycrystalline samples (about 5 g of each compound) for the present study were synthesized at the Institute for Solid State Physics (University of Tokyo) from high-purity starting materials using methods described earlier.[11] X-ray and neutron powder diffraction was used to confirm that they are the correct phases, nevertheless containing small amounts (% level) of impurity phases (Os, $AOsO_4$) whose contribution is negligible in the inelastic neutron scattering intensity. Inelastic neutron scattering experiments have been performed using the time-of-flight spectrometers IN4 and IN6 at the Institut Laue-Langevin, optimizing the experimental setup with respect to resolution and as a function of temperature of the observations. On IN6 we reach a resolution better than $\Delta(\hbar\omega) \lesssim 0.25$ meV (full width at half maximum, FWHM) in the energy-transfer range $-10\ \mathrm{meV} < \hbar\omega < -0.5\ \mathrm{meV}$ when operating with an incident wavelength of $\lambda_i = 4.14$ Å (4.77 meV). With this setup we can follow the temperature dependence down to $T \approx 50$ K with observation of neutron energy gain (anti-Stokes) response, however with the consequent drawback that lower temperatures observations are not feasible due to lack of thermal population. On IN4 operating with an incident neutron wavelength of $\lambda_i = 2.54$ Å (12.7 meV), an energy resolution of $\Delta(\hbar\omega) \approx 0.5$ meV (FWHM) was obtained in the range $1\ \mathrm{meV} < \hbar\omega < 10\ \mathrm{meV}$. Standard cryostats were used for temperature dependent measurements. Background correction with empty sample holder data and a vanadium calibration of the efficiency of the multidetector banks of the instruments were applied, then the data were converted to the experimental scattering function $S_{\mathrm{exp}}(Q,\omega)$. Due to the different incident wavelength and mode of operation the phase-space (Q,ω) range accessible on each of the instruments is different. Moreover, as it can be seen in Table I the atoms in these compounds are almost pure coherent scatterers; the observed intensity has a nontrivial Q-dependence that is averaged when using the incoherent approximation for the evaluation of the generalized density-of-states, see the details in the Appendix.

TABLE I. Coherent (σ_{coh}) and incoherent (σ_{inc}) neutron scattering cross sections in barns, atomic mass M, and total scattering power $[(\sigma_{\mathrm{coh}}+\sigma_{\mathrm{inc}})/M = \sigma_t/M]$ of the elements in the osmate samples studied.

Element	σ_c	σ_i	M	σ_t/M
K	1.71	0.25	39.1	0.050
Rb	6.3	0.3	85.5	0.077
Cs	3.69	0.21	133.0	0.029
Os	15.2	0.4	191.0	0.082
O	4.235	0	16.0	0.265

B. Powder averaged dynamic response

Inelastic neutron scattering gives a direct access to the dynamic response of the sample studied. On powder samples only the magnitude Q momentum-transfer vector $\mathbf{Q}$ can be defined when the energy transfer $\omega(Q)$ and the scattering angle 2θ are known. In our experiments using time-of-flight spectrometers a given detector positioned at an angle 2θ measures energy transfer and momentum-transfer dependent intensity $I(2\theta,\omega)$ that can be converted, after corrections of instrumental effects (see Sec. II A), to the scattering function $S(Q,\omega)$. From this experimental quantity we obtain the generalized neutron weighted density-of-states, see details in the Appendix. $S(Q,\omega)$ can be further interpolated on a constant Q grid. Accordingly one can examine the response at a constant length of Q. In favorable conditions it is then possible to select special Q values corresponding for example to low-order zone centers or zone boundaries which may help to identify specific features of the response.

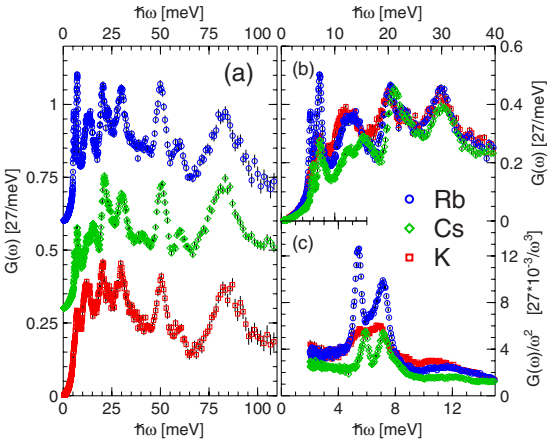

FIG. 1. (Color online) Panels (a) and (b): $G(\omega)$ of KOs_2O_6, $RbOs_2O_6$ and $CsOs_2O_6$ over the full and intermediate energy ranges, based on IN6 upscattering (anti-Stokes) data. In panel (a) the data points of the Cs and Rb compounds have been shifted up by 0.3 and 0.6, respectively, for clarity of presentation. Panel (c): $G(\omega)/\omega^2$ highlighting the low-energy double peaks. $G(\omega)$ has been normalized to 27 modes (3/atom of the formula unit) over the full energy range, see Eq. (A5).

III. EXPERIMENTAL RESULTS

A. Generalized density-of-states

Figure 1 shows the generalized density-of-states $G(\omega)$ of the three compounds measured at $T=300$ K on IN6. One can note the intense contribution at energies peaking at $\hbar\omega \approx 85$ meV, typical for oxygen modes in oxide compounds. Several peaked features appear at lower energies, at 60, 50, 30, 22, 13, and at $\hbar\omega \approx 7.5$ meV. A recent Raman work[21] on the K compound has shown prominent peaks at some of those positions, e.g., the ones in the vicinity of 240–260 cm^{-1} (30–32 meV) and at 490 cm^{-1} (60 meV). An additional peak is seen in $G(\omega)$ of $RbOs_2O_6$ and $CsOs_2O_6$ at even lower energy $\hbar\omega \approx 5.5$ meV while in KOs_2O_6 this feature is replaced by a weak shoulder. A double peak is clearly visible in the panel (c) of Fig. 1 that shows a plot of $G(\omega)/\omega^2$. In this plot one can also note that $G(\omega)/\omega^2$ is flat, almost constant in the lowest energy range $\hbar\omega \lesssim 4$ meV, characteristic of a Debye-type contribution where $G(\omega) \propto \omega^2$. The peaks in $G(\omega)$ mentioned above can be attributed to optical and/or zone-boundary modes with low value of group velocity $d\omega_j/dq \approx 0$. Following earlier work[20,21] we conclude that the prominent peaks at low-energy $\hbar\omega < 8$ meV are due to the motion of K, Rb, or Cs atoms. The relative intensity of the low-energy peaks is not too different from the ratio expected when considering the scattering power σ/M (σ is the total scattering cross section and M the atomic mass, see Table I). This quantity for individual atoms K, Rb, and Cs is roughly in proportion 5:8:3, while the integrals of the peaks in the Fig. 1, panel (c) have a ratio 5:9:3. We can note that in the earlier neutron work only a single peak was detected, partly due to lack of resolution and also because data were taken in at higher Q (2.4 $Å^{-1} \leq Q \leq$ 4.2 $Å^{-1}$) where the gap between the peaks tends to be filled with dispersive contributions and the Q-dependent intensity modulations are weaker and less distinguishable of the overall Q^2 dependence. Regarding these circumstances the data obtained in that study[20] at $T=300$ K are consistent with our observations.

B. Momentum-transfer dependence of the powder averaged response

The Q-dependent modulations of the phonon response illustrated in the Fig. 2 highlight the characteristic features of the phonon structure factor, Eq. (A6), due to the phase relations of the atomic motions of the distinct eigenmodes. Therefore it is possible to see the dispersive acoustic branches emanating from the Bragg-peak positions. Another consequence is modulation of the intensity of the rather nondispersive branches for which the mode energies remain flat, with weak group velocities $d\omega_j/dq \approx 0$. The Q dependence of the intensities can be examined in some detail using the data presented in Fig. 2. Constant energy-transfer strips of the response at $T=300$ K are shown in Fig. 3 for all three compounds. One can see that the Q dependence shows modulation on top of the overall Q^2 trend that is characteristic of the phonon response. We can also examine the quantity $g_{\mathrm{exp}}(Q,\omega)$ defined in the Appendix, Eq. (A4). As depicted in Fig. 4 for K and Rb compounds we can see that $g_{\mathrm{exp}}(Q,\omega)$ shows characteristic Q dependence. Especially worth noting is the systematic variation of the energy-transfer dependence seen at different values of Q which is clearly seen in the Rb compound, similar but not so marked in the K compound due to the much broader, less peaked response. In $RbOs_2O_6$ the higher energy band is at maximum for a momentum transfer $Q=1.1$ $Å^{-1}$, coinciding with the modulus of the [111] zone center, while for the lower band the maximum is seen at a $Q=1.6$ $Å^{-1}$, matching the $[\frac{3}{2}\frac{3}{2}\frac{3}{2}]$ zone boundary. These features bear some resemblance to the observations reported recently on the skutterudite compounds $(La,Ce)Fe_4Sb_{12}$ for which a detailed comparison with *ab initio* phonon response indicated that such features can result from the extended flat region of the top part of the acoustic branches and from weakly dispersive optical branches.[5]

C. Temperature dependence

The effects of cooling on the low-energy modes in all of the compounds are compiled in the Fig. 5 where we plot against temperature the positions of the maxima of the momentum-transfer averaged intensity. In $CsOs_2O_6$ and $RbOs_2O_6$ we observe a progressive softening while in KOs_2O_6 we see a steep change of the characteristic energy of the low-energy peak. In this compound the softening finally saturates below $T \lesssim 40$ K, giving a peaked band positioned at $\hbar\omega \approx 3.4$ meV in the lowest temperature range. We have shown in Fig. 5 the positions of the two clearly defined maxima for the Rb and Cs compounds. The situation appears to be more complicated in KOs_2O_6 as depicted in Fig. 6. Due to the increasing damping of the response on cooling the higher energy maximum becomes rapidly ill defined and therefore we only plot the lower maximum in Fig. 5. Moreover we can note that the T-dependent positions of the T_{2g}

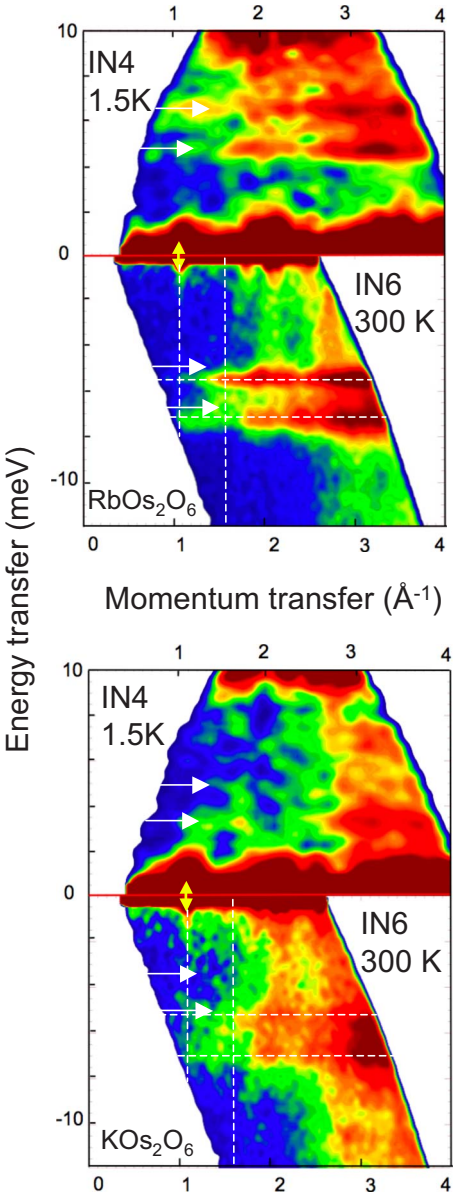

FIG. 2. (Color online) $S(Q,\omega)$ maps of KOs_2O_6 and $RbOs_2O_6$. For each panel the top part shows the Stokes data obtained at IN4 at $T=1.5$ K, the one below the anti-Stokes data obtained at IN6 at $T=300$ K. The split band at 5 meV$\lesssim|\hbar\omega|\lesssim$8 meV at $T=300$ K is softer at $T=1.5$ K (as shown by the white arrows). In KOs_2O_6 the low-T response is peaking at $\hbar\omega\approx3.4$ meV. The [111] zone center ($Q=1.07$ Å^{-1}) is marked with the vertical yellow arrow. The horizontal dashed lines indicate the constant energy cut positions of Fig. 3, the vertical ones those of the constant Q-cut positions of Fig. 4.

mode assigned in the Raman study[21] to the K-atom vibrations, located at 70 cm^{-1} (8.7 meV) at $T=300$ K and at about 62 cm^{-1} (7.7 meV) at $T=50$ K do not correspond to any strong features in the neutron response we have followed in the K compound, see Fig. 6, even though a small kink at $T=300$ K appears close to the expected position.

In a recent report,[19] motivated by the earlier calculations[12] and NMR observations[18] a model was proposed for the temperature dependence of the effective frequency of a localized

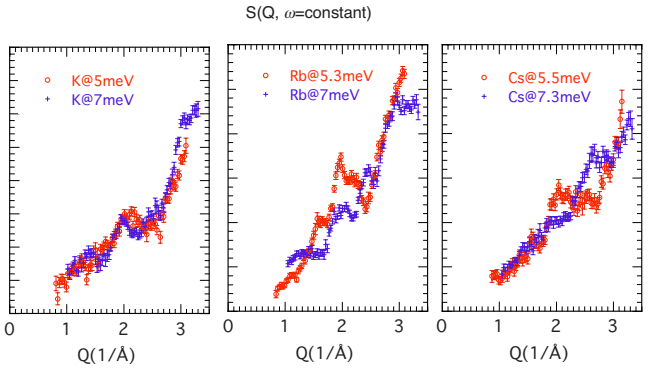

FIG. 3. (Color online) Constant energy Q dependence of KOs_2O_6, $RbOs_2O_6$, and $CsOs_2O_6$ at $T=300$ K along the positions of the low-energy bands at the values indicated on the plot, see Fig. 2. The vertical scale is arbitrary and not the same for all plots.

anharmonic phonon. The model predicts quantitatively the hardening of the phonon frequency on increasing temperature and in spite of the simplicity of the phonon model that was used, with respect to the situation we have observed, the prediction for the temperature dependence is qualitatively in agreement with our data, see Fig. 5. The dimensionless β parameter is a direct measure of the strength of the anharmonicity[19] and we can see that it depends on the alkali atom just as expected,[12] strongest for K and weakest for Cs. For the case of KOs_2O_6 a unique value of the anharmonicity parameter β is not adequate for the full T range, which might indicate temperature dependence of the potential.

IV. DISCUSSION

The low-energy features of the lattice dynamics observations reported here for the β pyrochlore compounds are consistent with the existing specific-heat results but point out certain quantitative shortcomings of the specific-heat analysis. The Einstein temperatures concluded from the thermodynamic data $\Theta_E=60$ and 70 K, for the Rb and Cs compounds,[8,10] respectively, match the average position of

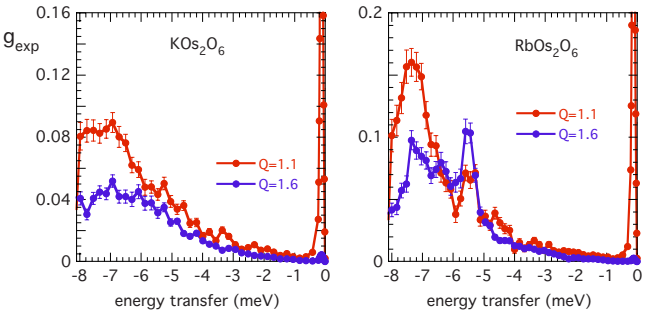

FIG. 4. (Color online) Constant-Q energy dependence of $g_{exp}(Q,\omega)$, Eq. (A4), for KOs_2O_6 and $RbOs_2O_6$ at $T=300$ K, at the Q positions of the [111] zone center ($Q=1.1\pm0.05$ Å^{-1}), and of the $[\frac{3}{2}\frac{3}{2}\frac{3}{2}]$ zone boundary ($Q=1.6\pm0.05$ Å^{-1}), see Fig. 2. The vertical scale is arbitrary. The high values seen at $Q=1.1$ Å^{-1} close to zero energy are due to the elastic scattering from the 111 Bragg peak.

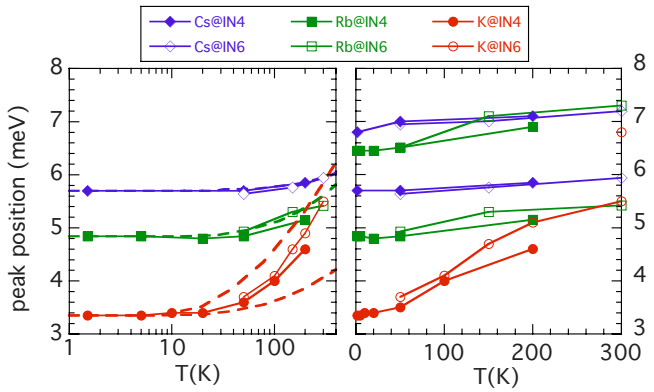

FIG. 5. (Color online) T dependence of the maxima of the low-energy peaks for the Cs, Rb, and K compounds, lines are guides for the eye. For KOs_2O_6 we plot the upper peak position only at $T=300$ K as the higher energy peak becomes poorly defined on cooling, see Fig. 6. The left panel with log(T) scale highlights the level of the lower band positions (only those are shown for clarity) at low T, including a comparison with the theory of Dahm and Ueda (Ref. 19) shown by the dashed lines calculated with the anharmonicity parameters $\beta=0.1$, 1, $\beta=0.1$, and $\beta=0.025$ for K, Rb, and Cs compounds, respectively.

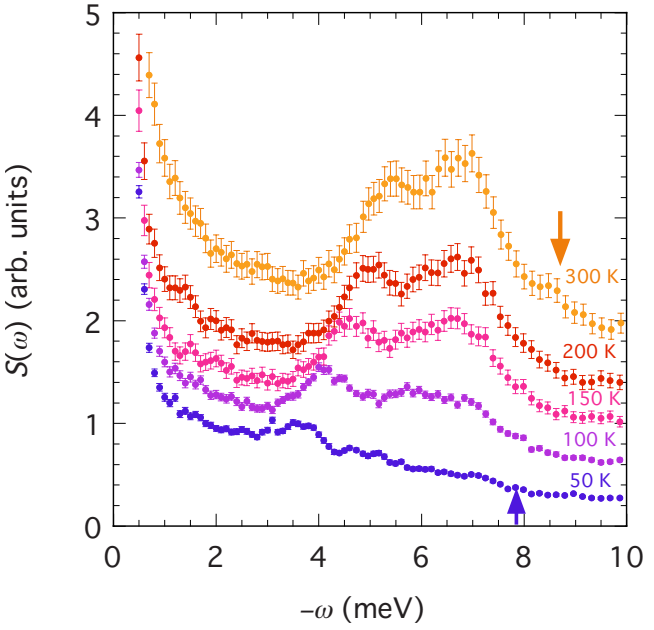

FIG. 6. (Color online) T dependence of the momentum-transfer integrated low-energy anti-Stokes response in KOs_2O_6. In spite of the increasing damping the softening on cooling of the lower energy maximum is rather well defined, while the position of the higher energy maximum is less clear and a shoulder persists with an almost temperature independent position at about $\hbar\omega\approx 7$ meV. The position at $T=50$ and 300 K of the T_{2g} mode observed in the Raman study (Ref. 21) is indicated by the vertical arrows.

the prominent peaked response we have observed in low-energy, low-T dynamic response. The case of KOs_2O_6 is more complicated due to the strong temperature dependence of the low-energy phonon modes. All this points out that the phenomenological models with T-independent parameters cannot unambiguously describe the specific-heat data over an extended T range, explaining in part why the Einstein temperatures cited for the potassium compound range from $30\ \text{K}\leq\Theta_E\leq 40$ K with one mode[8,11] or give two modes[10] with $\Theta_E=22$ and 60 K. We must stress that the specific-heat analysis is not sensitive enough to discern the fine details of the phonon spectrum and inadequate for observing the temperature dependence of the phonon frequencies and the anharmonicity that could be associated with the 'rattling' character.

A clear outcome of the present study is the failure of the quasiharmonic lattice dynamics evidenced by the nontrivial temperature dependence of the split phonon band energies. Anharmonicity occurring in any solid usually softens the phonons on heating due to the weakening of the potential for increasing vibrational amplitude. On the contrary we observe a hardening of the phonons on increasing temperature and the associated increase of the vibrational amplitude. Such an effect can be qualitatively understood by considering a flat bottom or steep walls potential in which the effective force constant increases rapidly for increasing displacement amplitude. This might not be surprising in view of the earlier computational work but it is nevertheless the first experimental evidence on this anharmonic behavior in the osmates.

Among the three osmate compounds we have studied KOs_2O_6 stands out due to its strong anharmonicity and damping of the phonon response that is visible as considerable temperature dependent broadening of the phonon peaks, see Fig. 6. These observations remind on those clathrate hydrates for example[22] and could be relevant to the question of the localization of the K atom and its possible off centering.[17] In the computational work[13] it was suggested that the peculiarity of the K compound with respect to the Rb and Cs counterparts stems from stronger intersite coupling. The dynamical simulations concluded that particular high amplitude vibrational modes associated with the anisotropic fourfold potential of the K atom interacting with its nearest-neighbor K sites could lead to a complex displacement pattern that freezes at the phase transition observed on single-crystal samples. Our observations of the Q dependence of the response at $T=300$ K, Figs. 3 and 4, show a local maximum in the vicinity of the [111] zone center that was not predicted in the theoretical study based on a finite cluster calculation.[13] Moreover, we have seen that the Q-dependent features are sharper in the Rb compound. This suggests that the collective behavior is somehow similar but smeared due to damping in the K counterpart. Anyhow it is interesting to note that the strong response of at $Q=1.1$ Å^{-1} corresponding to the [111] zone center, Fig. 4, is consistent with a high amplitude longitudinal mode with displacement toward the nearest-neighbor A atom.

Based on the present results we cannot make any definitive conclusions concerning the conjectured ground state of the KOs_2O_6 compound. In addition we have not observed any particular changes of the mode energy of the K compound to happen across the superconducting T_c which is in clear contradiction with the ideas proposed in a recent paper.[23] Detailed calculations of the lattice dynamics are needed to characterize the low-energy phonon properties from the powder averaged response, along the lines used in the work on skutterudites.[5]

To summarize we have investigated, using inelastic neutron scattering on powder samples, the lattice dynamics of the β-pyrochlore compounds KOs_2O_6, $RbOs_2O_6$, and $CsOs_2O_6$. In all of them we have observed a low-energy response with quantitatively different temperature dependence for the different compounds. Our results, with a split flat phonon band in this energy range and collective phase coherence of the vibrations, indicate a situation more complicated than the single-particle "rattling" supposed earlier. Comparing with a recently proposed model[19] the relative strength of anharmonicity of the flat phonon bands in KOs_2O_6, $RbOs_2O_6$, and $CsOs_2O_6$ follows the trend expected from the previous calculations.[12] The role of the particular dynamic response in the superconducting properties[10] and in association with the ground-state structure[17] needs further studies. Moreover, these compounds merit further attention in the general framework of "rattling modes" of encaged atoms.

ACKNOWLEDGMENTS

We wish to thank K. Ueda for a useful discussion as well as C. Ritter for checking composition and phase purity of the samples with neutron powder diffraction.

APPENDIX: PHONON-SCATTERING FUNCTION AND NEUTRON WEIGHTED DENSITY-OF-STATES

In the case of coherent phonon scattering from multielement system it is possible to define the neutron weighted, generalized density-of-states $G(\omega)$ as an average over the momentum transfer[24–27] (the presentation follows closely the one of Ref. 27, for basic concepts see Ref. 28)

$$G(\omega) = \frac{1}{\Delta Q'} \int_{Q'}^{Q'+\Delta Q'} g_{\text{eff}}(Q,\omega) dQ. \tag{A1}$$

In this expression

$$g_{\text{eff}}(Q,\omega) = \int g_{\text{eff}}(\mathbf{Q},\omega) d\mathbf{\Omega}_{\mathbf{Q}} \tag{A2}$$

is the powder average of the quantity

$$g_{\text{eff}}(\mathbf{Q},\omega) = \frac{2\bar{M}\ \exp(2\bar{W}_Q)}{\hbar Q^2} \omega S(\mathbf{Q},\omega) \left[1 - \exp\left(-\frac{\omega}{k_B T}\right)\right] \tag{A3}$$

in which the average mass and the average Debye-Waller factor are defined by $\bar{M}^{-1} = N^{-1}\Sigma_i m_i^{-1}$, $\bar{W}_{\mathbf{Q}} = N^{-1}\Sigma_i W_i(\mathbf{Q})$, and the index i runs over all atoms. Based on this formalism the experimental evaluation of the density-of-states proceeds by noting that the quantity $S_{\text{exp}}(Q,\omega)$ measured on a polycrystalline powder is the powder average of the product of the scattering function and the Debye-Waller factor. In order to obtain the experimental neutron weighted density-of-states we use Eq. (A1), replacing $g_{\text{eff}}(Q,\omega)$ by the measured quantity

$$g_{\text{exp}}(Q,\omega) = \frac{\omega}{Q^2} S_{\text{exp}}(Q,\omega) \left[1 - \exp\left(-\frac{\omega}{k_B T}\right)\right]. \tag{A4}$$

Note that we drop here the factor $\bar{M}/\hbar$ because experimental $G(\omega)$ is usually obtained without absolute units while it is instead normalized to the number of modes, $3N'$ for each of the n distinct atoms in N' formula units or unit cells. This normalization is approximate due to the fact that the experimentally obtained, generalized, or neutron weighted density-of-states is different from the true vibrational density-of-states

$$g(\omega) = \sum_{i=1}^{n} g_i(\omega) = \sum_{i=1}^{n} \frac{1}{3N'} \sum_{j=1}^{3N'} \delta(\omega - \omega_{i,j}) \tag{A5}$$

since the experimental quantity contains the partial contributions of the individual atoms weighted by their scattering power[22] σ_i/M_i, and by consequence there is a ω-dependent factor relating the two. The σ_i/M_i dependence is evident when considering the expression for the structure factor (note that $\sigma_i = 4\pi b_i^2$)

$$|F_i(\mathbf{Q})|^2 = \sum_{k,l} \frac{\overline{b_k b_l}}{\sqrt{m_k m_l}} e^{[W_k(\mathbf{Q}) - W_l(\mathbf{Q})]} [\mathbf{Q} \cdot \mathbf{e}_j(k)] \times [\mathbf{Q} \cdot \mathbf{e}_j(l)] e^{i(\mathbf{Q}\cdot\mathbf{r}_k - \mathbf{Q}\cdot\mathbf{r}_l)} \tag{A6}$$

that enters in the single phonon-scattering function

$$S(\mathbf{Q},\omega) = \frac{1}{2N\langle\overline{b^2}\rangle} \sum_j \frac{|F_j(\mathbf{Q})|^2}{\omega_j} [\delta(\omega - \omega_j) - \delta(\omega + \omega_j)] \times \left[1 - \exp\left(-\frac{\omega_j}{k_B T}\right)\right]. \tag{A7}$$

For the crystalline systems the Eqs. (A6) and (A7) can be simplified taking into account the periodic arrangement of the atomic positions.[28] Another reason for the difference between the experimental $G(\omega)$ and the true $g(\omega)$ is the $\mathbf{Q}$ dependence of the structure factor in the Eq. (A6). The usual way out from this problem is to apply a broad enough Q range and rather elevated values of Q in the experimental averaging in order to cover several Brillouin zones. On the other hand when operating in the region of low-order zone centers or zone boundaries of the reciprocal space it is possible to distinguish contributions that can reflect characteristic features of the coherent dynamic structure factor of Eq. (A6). A correction can be applied to remove the broad continuous multiphonon-scattering response that extends beyond the single phonon cutoff.[29] This was not done in the present analysis.

*mutka@ill.fr

[1] B. C. Sales, D. Mandrus, B. C. Chakoumakos, V. Keppens, and J. R. Thompson, Phys. Rev. B **56**, 15081 (1997).
[2] V. Keppens, D. Mandrus, B. C. Sales, B. C. Chakoumakos, P. Dai, R. Coldea, M. B. Maple, D. A. Gajewski, E. J. Freeman, and S. Bennington, Nature (London) **395**, 876 (1998).
[3] R. P. Hermann, R. Jin, W. Schweika, F. Grandjean, D. Mandrus, B. C. Sales, and G. J. Long, Phys. Rev. Lett. **90**, 135505 (2003).
[4] M. Christensen, F. Juranyi, and B. B. Iversen, Physica B (Amsterdam) **385-386**, 505 (2006).
[5] M. M. Koza, M. R. Johnson, R. Viennois, H. Mutka, L. Girard, and D. Ravot, Nature Mater. **7**, 805 (2008).
[6] M. Koza, M. Johnson, R. Viennois, H. Mutka, L. Girard, and D. Ravot, in XXV International Conference on Thermoelectrics, edited by M. Rotter (IEEE, Vienna, 2006), Catalog No. 06TH8931, p. 71.
[7] M. Brühwiler, S. M. Kazakov, N. D. Zhigadlo, J. Karpinski, and B. Batlogg, Phys. Rev. B **70**, 020503(R) (2004).
[8] M. Brühwiler, S. M. Kazakov, J. Karpinski, and B. Batlogg, Phys. Rev. B **73**, 094518 (2006).
[9] T. Shibauchi *et al.*, Phys. Rev. B **74**, 220506(R) (2006).
[10] Z. Hiroi, S. Yonezawa, Y. Nagao, and J. Yamaura, Phys. Rev. B **76**, 014523 (2007).
[11] Z. Hiroi, S. Yonezawa, T. Muramatsu, J.-I. Yamaura, and Y. Muraoka, J. Phys. Soc. Jpn. **74**, 1255 (2005).
[12] J. Kuneš, T. Jeong, and W. E. Pickett, Phys. Rev. B **70**, 174510 (2004).
[13] J. Kuneš and W. E. Pickett, Phys. Rev. B **74**, 094302 (2006).
[14] Y. Shimono, T. Shibauchi, Y. Kasahara, T. Kato, K. Hashimoto, Y. Matsuda, J. Yamaura, Y. Nagao, and Z. Hiroi, Phys. Rev. Lett. **98**, 257004 (2007).
[15] T. Shimojima *et al.*, Phys. Rev. Lett. **99**, 117003 (2007).
[16] Z. Hiroi, S. Yonezawa, J.-I. Yamaura, T. Muramatsu, and Y. Muraoka, J. Phys. Soc. Jpn. **74**, 1682 (2005).
[17] R. Galati, C. Simon, P. F. Henry, and M. T. Weller, Phys. Rev. B **77**, 104523 (2008).
[18] M. Yoshida, K. Arai, R. Kaido, M. Takigawa, S. Yonezawa, Y. Muraoka, and Z. Hiroi, Phys. Rev. Lett. **98**, 197002 (2007).
[19] T. Dahm and K. Ueda, Phys. Rev. Lett. **99**, 187003 (2007).
[20] K. Sasai, K. Hirota, Y. Nagao, S. Yonezawa, and Z. Hiroi, J. Phys. Soc. Jpn. **76**, 104603 (2007).
[21] T. Hasegawa, Y. Takasu, N. Ogita, M. Udagawa, J. I. Yamaura, Y. Nagao, and Z. Hiroi, Phys. Rev. B **77**, 064303 (2008).
[22] H. Schober, H. Itoh, A. Klapproth, V. Chihaia, and W. F. Kuhs, Eur. Phys. J. E **12**, 41 (2003).
[23] J. Chang, I. Eremin, and P. Thalmeier, arXiv:0803.2491 (unpublished).
[24] J. M. Carpenter and C. A. Pelizzari, Phys. Rev. B **12**, 2391 (1975).
[25] J. M. Carpenter and C. A. Pelizzari, Phys. Rev. B **12**, 2397 (1975).
[26] D. L. Price and J. M. Carpenter, J. Non-Cryst. Solids **92**, 153 (1987).
[27] S. N. Taraskin and S. R. Elliott, Phys. Rev. B **55**, 117 (1997); it appears that a factor ω is missing in Eqs. (7) and (8) of this article.
[28] G. L. Squires, *Introduction to Thermal Neutron Scattering* (Dover, New York, 1996).
[29] H. Schober, J. Phys. IV **103**, 173 (2003).